1-1-2008

Theory and simulation of surface plasmon excitation using resonant metal nanoparticle arrays

Amitabh Ghosal
University of Central Florida

Pieter G. Kik
University of Central Florida

Theory and simulation of surface plasmon excitation using resonant metal nanoparticle arrays

Cite as: J. Appl. Phys. **103**, 113111 (2008); https://doi.org/10.1063/1.2936971
Submitted: 29 October 2007 . Accepted: 29 March 2008 . Published Online: 12 June 2008

Amitabh Ghoshal, and Pieter G. Kik

Theory and simulation of surface plasmon excitation using resonant metal nanoparticle arrays

Amitabh Ghoshal[a] and Pieter G. Kik[b]
CREOL, The College of Optics and Photonics, University of Central Florida, 4000 Central Florida Blvd., Orlando, Florida 32816, USA

(Received 29 October 2007; accepted 29 March 2008; published online 12 June 2008)

We discuss a plasmonic coupling device consisting of a periodic array of ellipsoidal silver nanoparticles embedded in SiO_2 and placed near a silver surface. By tuning the shape of the particles in the array, the nanoparticle plasmon resonance is tuned. The resulting resonantly enhanced fields near the nanoparticles, in turn, excite surface plasmons on the metal film. We have performed finite integration technique simulations of such a plasmon coupler, optimized for operation near a wavelength of 676 nm. Analysis of the frequency dependent electric field at different locations in the simulation volume reveals the separate contributions of the particle and surface resonance to the excitation mechanism. A coupled oscillator model describing the nanoparticle and the metal film as individual resonators is introduced and is shown to reproduce the trends observed in the simulations. Implications of our analysis on the resonantly enhanced excitation of surface plasmons are discussed. © *2008 American Institute of Physics*. [DOI: 10.1063/1.2936971]

I. INTRODUCTION

In recent years, there has been a rapid growth in research on surface plasmon nanophotonics.[1] Surface plasmons are electron charge density waves that can exist at a metal surface or at the interface between a metal and a dielectric.[2] The propagating electromagnetic modes associated with surface plasmons can be strongly confined, making surface plasmons on metal films possible candidates for nanoscale optical waveguides.[3–11] Several designs have been successfully realized, including waveguides comprised of metal stripes,[12] wedges,[6] and gaps[5] in metal films and strip-loaded surface plasmon waveguides.[3] Using surface plasmons on metal films and waveguides, passive components such as Bragg reflectors,[13] ring resonators,[14] and Y-splitters,[14] as well as active components such as Mach–Zehnder interferometer based switches[15] have been realized. Despite the vast amount of work on these components, the development of an integrated surface plasmon source remains a challenge. As a result, light is commonly introduced into nanophotonic circuits by coupling external radiation into bound modes.[16–19] This approach faces some of the same challenges as the excitation of optical modes in dielectric waveguides; since the wavevector of the guided surface plasmon modes exceeds that of externally incident light at any incident angle, it is not generally possible to directly excite guided surface plasmons with far-field light. A common method of exciting surface plasmons is prism coupling using either the Kretschman[2] or Otto[2] geometry. In this approach, phase matching with surface plasmons is achieved by increasing the wavevector of the incident light using a high dielectric constant material placed in close proximity to the metal waveguide surface. The excitation efficiency using this approach can be close to unity using broad area illumination. A second approach involves grating coupling, in which a periodic corrugation of the metal surface (or a nearby interface) is used to overcome the momentum mismatch between free-space light and the surface plasmon modes.[2] Excitation of surface plasmons with close to unit efficiency has also been demonstrated using illumination of relatively large grating couplers with a high number of grating periods.[2] A final common approach for surface plasmon excitation involves the use of isolated nanostructures on or near a metal surface. For example, surface plasmons have been excited using a near-field scanning optical microscopy tip,[20] random surface roughness,[21] as well as intentionally created features such as metal nanoparticles[22] and lines[22] on or near[23,24] a metal film, holes in metal films,[25–27] and edges of metal films.[28]

In this paper we consider the use of localized plasmon resonances for the excitation of surface plasmons using two-dimensional arrays of metal nanoparticles placed near a metal-dielectric interface. A schematic of such a structure is shown in Fig. 1. This combination of resonant nanoparticle based surface plasmon excitation and grating coupling may be used to design compact free-space to surface plasmon couplers as well as field enhancement structures. Ellipsoidal metal nanoparticles exhibit a dipolar surface plasmon resonance known as the Fröhlich mode[29] at a frequency that de-

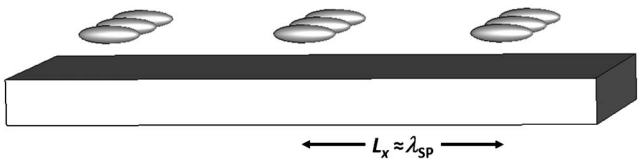

FIG. 1. A schematic of a section of an infinite array of ellipsoidal silver nanoparticles, embedded in silica, and above an extended silver film.

[a]Author to whom correspondence should be addressed. Electronic mail: aghoshal@mail.ucf.edu.
[b]Also at Physics Department, University of Central Florida, Orlando, FL 32816.

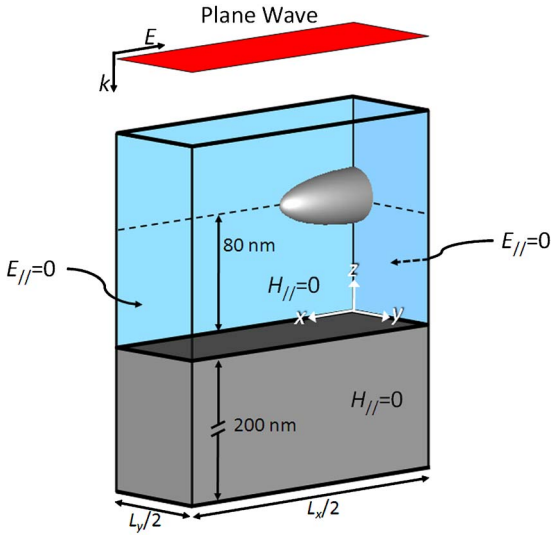

FIG. 2. (Color online) A schematic of the simulated plasmon excitation structure. Gray regions correspond to silver, and the blue regions correspond to silica.

pends on the particle aspect ratio, its dielectric function, and the dielectric function of its surroundings. The resonantly enhanced localized field distribution that can be excited on individual metal nanoparticles contains high spatial frequency components that can couple to propagating surface plasmons on a nearby metal film. By placing such resonant particles in a periodic arrangement near a metal film, surface plasmons excited by multiple particles can be added constructively, resulting in an enhanced surface plasmon excitation efficiency. In this work we numerically investigate excitation of surface plasmons on a silver film using an infinitely extended two-dimensional array of metal nanoparticles near a metal film. The excited surface plasmon amplitude is studied as a function of excitation frequency and nanoparticle aspect ratio. The results are compared to an analytical model that describes the silver surface and the metal nanoparticles as coupled resonators. We find that the main features observed in three-dimensional full-field simulations are well described by this coupled oscillator model. Our results show that the strong coupling between the incident light, the resonant nanoparticles, and the silver surface results in anticrossing behavior and a reduced surface plasmon coupling efficiency when the individual particle and surface resonance frequencies are approximately equal. Implications for the design of field enhancement structures and surface plasmon couplers are discussed.

II. SIMULATION PARAMETERS

The structure under investigation consists of an array of ellipsoidal silver nanoparticles placed in close proximity to a silver surface. The electromagnetic response of the system was studied using the finite integration technique[30] (FIT) as implemented in CST Microwave Studio.[31] A schematic of the simulation volume is shown in Fig. 2. The system consists of a 200 nm thick silver film extended infinitely in the x-y plane, embedded in SiO_2. The silver film thickness is chosen to prevent measurable coupling of surface plasmon amplitude from the top to the bottom surface of the film. An ellipsoidal silver nanoparticle of semiaxes $a \times b \times c$ along the x-, y-, and z-directions, respectively, is located in the SiO_2 host with the center of the nanoparticle placed 80 nm above the metal surface. The particle aspect ratio $AR=a/c$ with $b=c$ is varied between 2 and 4 while keeping the particle volume fixed and equal to the volume of a 30 nm diameter spherical nanoparticle. The particle volume is maintained constant to exclusively investigate shape related effects and to eliminate volume related changes in resonance frequency and amplitude. The system is excited at normal incidence using a plane wave polarized along the x-direction and traveling in the negative z-direction. Electric boundary conditions (tangential electric field components zero) were applied at $x=0$ and at $x=L_x/2$, while magnetic boundary conditions (tangential magnetic field components zero) were applied at $y=0$ and $y=L_y/2$. Here L_x and L_y are size parameters that describe the simulation geometry. Open boundary conditions were applied along the positive and negative z-directions. These boundary conditions together effectively simulate an infinite array of nanoparticles with a longitudinal spacing of L_x and a lateral spacing of L_y above an infinitely extended silver film. The temporal dependence of the excitation signal was chosen to be a Gaussian modulated sine wave centered at a free-space wavelength of 676 nm (4.35×10^{14} Hz) with a pulse duration of 16 fs. This corresponds to a wavelength range from 451 nm (6.65×10^{14} Hz) to 1357 nm (2.21×10^{14} Hz). The center wavelength was chosen to coincide with an experimentally available laser wavelength; however, the trends observed in the simulations do not depend on the exact center wavelength chosen. For example, a similar particle based coupler can be designed at 850 nm, a standard short range optical communications wavelength. For the present study, the lateral particle spacing was chosen to be $L_y=100$ nm, and the longitudinal interparticle spacing was set to $L_x=440$ nm. This length was chosen to coincide with the calculated $Ag-SiO_2$ surface plasmon wavelength at a free-space wavelength of 676 nm. The frequency dependent complex dielectric function of silver was described using a Drude model fit to available literature values.[32] The real part of the modeled permittivity differed from the experimental data[32] by less than 6% across the simulation bandwidth, while the imaginary part of the permittivity was set equal to the known literature value at the design frequency. Since the silver dielectric function deviates from the idealized Drude response, the imaginary part of the dielectric function differs from the literature values[32] by up to a factor 2 in the frequency range used. The dielectric constant of SiO_2 was set to a constant value of $\varepsilon_r=2.21$ over the entire wavelength range of the simulation. Due to the high dielectric contrast in metallodielectric nanostructures, extremely small mesh sizes are required in order to ensure convergence.[33] In this study mesh cell sizes ranging from 1 to 4 nm were used near metal-dielectric interfaces. Mesh convergence tests showed that the resulting errors in the electric field magnitude and resonance frequency values in this work are $\pm 2.5\%$ and $\pm 0.2\%$, respectively.

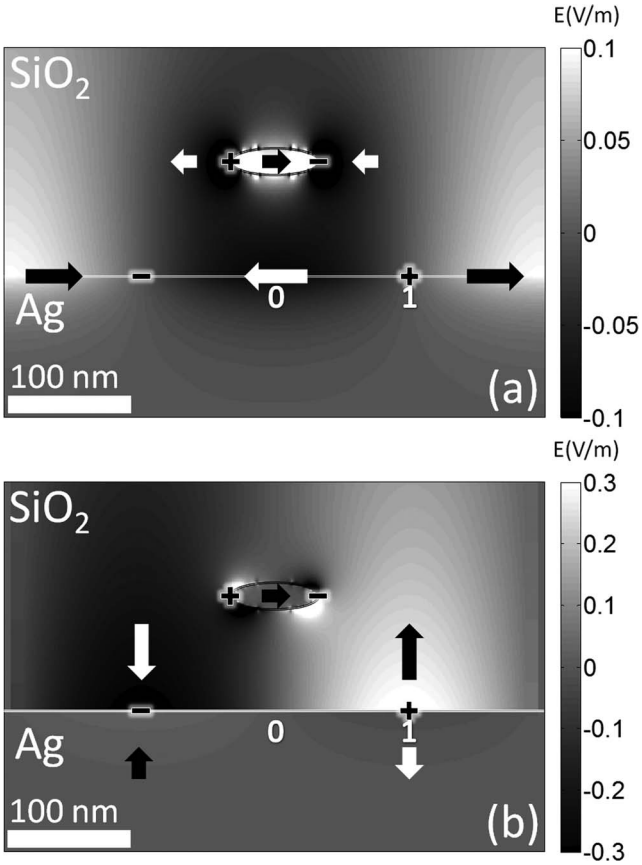

FIG. 3. (a) $E_x(x,z)$ and (b) $E_z(x,z)$ fields at $y=0$ at a time $t=59$ fs. The arrows indicate the direction of the field, and the location of the corresponding surface charges is indicated schematically. The field values displayed were limited to ± 0.1V/m for (a) and ± 0.3V/m for (b) to show the salient features of the structure.

III. SIMULATION RESULTS

Figure 3 shows the distribution of the x and z components of the electric field (E_x and E_z) in the simulation volume at $y=0$, for an ellipsoidal particle with an AR of 3.5 at time $t=59$ fs. Several important features are observed. First, note that E_z is maximum near the film surface at locations $x=-L_x/4$ and $x=+L_x/4$ (labeled location 1) and changes sign around the film surface. This is indicative of the presence of surface charge. At the metal surface the corresponding E_x amplitude is found to show a local maximum at $x=0$ underneath the particle (labeled location 0) as well as at $-L_x/2$ and $L_x/2$. Both these observations point to the presence of surface plasmons. Second, the observed E_x and E_z field distributions observed around the particle indicate a predominantly dipolar polarization of the particle. The charge distribution responsible for the observed fields at the film surface and near the particle is indicated schematically by the + and − signs in Fig. 3.

In order to obtain a measure for the excited surface plasmon amplitude on the metal film, we monitor the E_z amplitude just above the metal film ($z=1$ nm) at position 1. Note that at this position the particle dipole field adds a finite E_z contribution. The time evolution of E_z at location 1 is shown in Fig. 4(b). Although the excitation signal can be seen to end at time 0.016 ps in Fig. 4(a), extended ringing of E_z is observed well after the excitation signal has passed, indicating the existence of electromagnetic resonances on the system. Note that the full FIT simulation extended for 0.75 ps in order to allow the energy in the system to decay to negligible levels (below −40 dB of the maximum energy). Figure 5 displays the Fourier transform of this time-domain signal, normalized to the Fourier transform of the incident pulse. Two clear resonances with markedly different linewidths are observed. The narrow resonance at 4.35×10^{14} Hz lies close to the theoretical Ag−SiO_2 surface plasmon frequency for a surface plasmon that has a wavevector $k_{SP,x}=2\pi/L_x$ which occurs at $f=4.44\times10^{14}$ Hz based on the dielectric functions used. Consequently, this resonance is attributed to the constructive interference of surface plasmons excited along the x-direction by the nanoparticles. The full width at half maximum of this resonance is found to be 2.0×10^{12} Hz. This sharp resonance will be referred to as the *film resonance* in this work. The broader resonance at 3.7×10^{14} Hz lies close to the analytically calculated nanoparticle resonance frequency of 3.81×10^{14} Hz for an isolated silver particle with an AR of 3.5 embedded in SiO_2. This resonance will be referred to as the *particle resonance* in this work. Note that since the signal shown in Fig. 5 is normalized to the Fourier

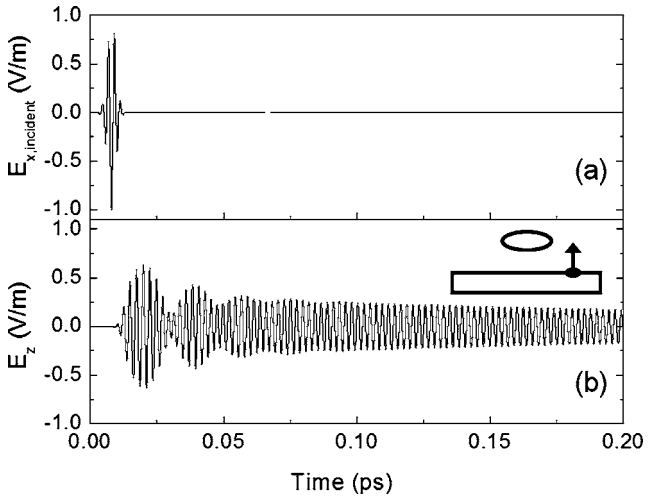

FIG. 4. (a) Time dependence of the plane-wave excitation amplitude at the input of the simulation volume. (b) Time evolution of the E_z field at location 1 (vertical arrow in inset) for a particle aspect ratio of 3.5.

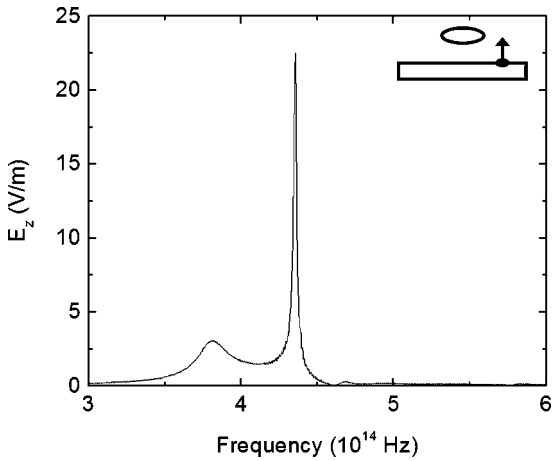

FIG. 5. Fourier transform of the time domain E_z signal observed at location 1 (vertical arrow in inset) for a particle aspect ratio of 3.5.

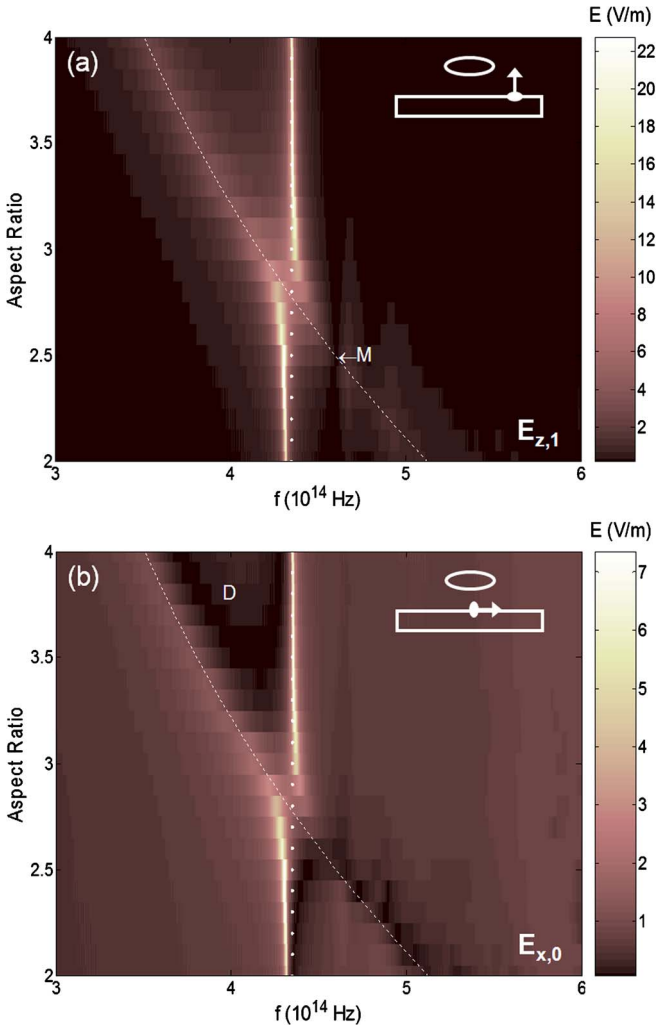

FIG. 6. (Color online) Electric field magnitude (a) $|E_z(f)|$ at location 1, and (b) $|E_x(f)|$ at location 0, as obtained from the simulations, for particle aspect ratios in the range of 2–4. The probe locations are schematically indicated.

transform of the excitation signal, field amplitudes larger than 1 are indicative of local field enhancement.

To study the influence of the particle resonance frequency on the surface plasmon excitation, the calculation shown in Fig. 5 was repeated for aspect ratios in the range of 2–4 (in steps of 0.1) corresponding to single particle resonance frequencies in the range of $(5.13-3.51)\times10^{14}$ Hz, as obtained by a separate set of FIT simulations. The resulting E_z magnitude at location 1 (predominantly surface plasmon related) as a function of frequency and particle aspect ratio is shown in Fig. 6(a), with color representing field amplitude as indicated by the scale bar. The location of the silver-SiO_2 film resonance at 4.35×10^{14} Hz is indicated by the vertical dotted line. As the aspect ratio of the particle is increased from 2 to 4, the resonance frequency associated with the nanoparticle (broad feature) is seen to decrease from 5.2×10^{14} to 3.6×10^{14} Hz. This is in correspondence with the expected response of an ellipsoidal particle excited with the electric field oriented along its long axis. For comparison, the dashed white line in Figs. 6(a) and 6(b) indicates the resonance frequency of an isolated Ag particle in SiO_2 calculated independently using FIT simulations. The observed full width at half maximum (FWHM) of the particle resonance is found to be 3.0×10^{13} Hz, which is close to experimentally observed damping of approximately 6×10^{13} Hz for similarly sized silver nanoparticles.[34] As the particle resonance frequency approaches the film resonance at AR≈2.9, a shift in the film resonance frequency as well as in the particle resonance frequency is observed. This shifting of resonances and the resulting anticrossing is typical of strongly coupled resonant systems. Note that as a result of this strong coupling the maximum field amplitude is *not* achieved when nanoparticle resonance and film resonance are identical. A final point of interest is the appearance of a field amplitude minimum (labeled *M*) at a frequency of 4.61×10^{14} Hz for all aspect ratios. Figure 6(b) shows the corresponding E_x field amplitudes obtained at location 0. The field at this location contains several field contributions: a contribution from the incident *x*-polarized wave, a contribution from the dipolar near-fields around the particle, a contribution due to the finite surface plasmon amplitude at the film surface, and fields due to any induced image charges. Similar trends are observed as in Fig. 6(a), including a clear signature of the particle and film resonances and evidence for anticrossing. However, notable differences are observed. For example, contrary to observations in Fig. 6(a), an area of reduced field amplitude is seen at high AR values (dark area labeled *D*). In addition, the sharp minimum observed in Fig. 6(a) is not observed in the E_x amplitude on the high frequency side of the film resonance. These differences will be discussed in greater detail in the Discussion.

Figure 6 shows that a particle AR of 2.9 leads to strong coupling and the appearance of two eigenmodes at different frequencies. In this strong coupling regime, the nanoparticle oscillation and the surface plasmon mode can no longer be considered independent resonances. Instead, two distinct eigenmodes exist. The nature of the eigenmodes is shown in Fig. 7, which shows the spatial distribution E_x at a fixed phase at $y=0$ for AR=2.9 at frequencies of (a) 4.23×10^{14} Hz and (b) 4.38×10^{14} Hz, respectively, corresponding to the two frequencies of maximum amplitude at this aspect ratio. The charge distribution associated with these field distributions is indicated schematically by the + and − signs. For the low energy mode at 4.23×10^{14} Hz shown in Fig. 7(a), the charge displacements at the nanoparticle location and at the film surface are seen to be antiparallel, corresponding to an out-of-phase oscillation of the charges in the particle and the film. For the high frequency mode shown in Fig. 7(b), the charge distribution of the nanoparticle and the surface plasmon are seen to be parallel, corresponding to in-phase oscillation of the charges. The observation of anticrossing, the appearance of field minima at distinct frequencies, and the nature of the observed eigenmodes can be understood in terms of a coupled oscillator model as described below.

IV. COUPLED OSCILLATOR MODEL

In order to gain insight into the origin of the features observed in Figs. 6(a) and 6(b), we developed a coupled oscillator model of the nanoparticle enhanced coupler. In this model, the nanoparticle is modeled as a driven Lorentz os-

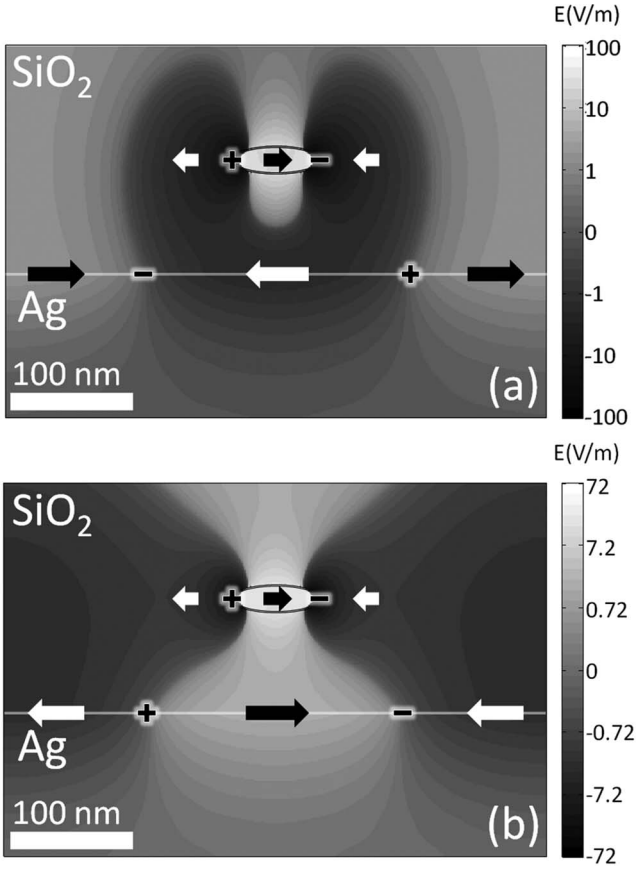

FIG. 7. $E_x(x,z)$ eigenmodes at $y=0$ at frequencies (a) 4.23×10^{14} Hz and (b) 4.38×10^{14} Hz at a particle aspect ratio of 2.9. The location of the corresponding charge distribution is indicated schematically.

cillator with a resonance frequency f_p that is determined by the nanoparticle aspect ratio. The time dependent field amplitude at the particle center is given by $E_p(t)$. The surface plasmon related film resonance associated with the surface plasmon present at the Ag–SiO_2 interface occurs at a well defined frequency due to the periodic nature of the system, and is modeled as a Lorentz oscillator with a fixed resonant frequency f_f. The time dependent field amplitude at location 0 is given by $E_f(t)$. The nanoparticle oscillator is driven by the incident radiation with corresponding electric field contribution $E_{\text{in}}(t)$, as well as by any E_x contribution due to surface plasmons on the metal surface. Electric fields due to image charges are not considered in this calculation since, near the resonances of interest, we expect the resonantly excited fields to exceed the magnitude non-resonant of image charge related fields. The resulting time dependent x-component of the electric field related to the polarization of the nanoparticle $E_p(t)$ is given by

$$\frac{\partial^2 E_p(t)}{\partial t^2} + \Gamma_p \frac{\partial E_p(t)}{\partial t} + \omega_p^2 E_p(t) = -A[E_{\text{in}}(t) + C_{\text{fp}} E_f(t)], \tag{1}$$

where Γ_p is the effective damping constant of the particle resonance including radiative damping, ω_p represents the resonance frequency of the nanoparticle in rad/s, the parameter A is a proportionality factor that depends on the particle resonance, and C_{fp} is a coupling constant ranging from 0 to 1 relating the surface plasmon field strength at the film surface to the field strength at the particle location. The magnitude of the parameter A can be estimated by realizing that at low frequencies, and neglecting any film contribution, the total field in the conductive nanoparticle tends to zero or $E_p \approx -E_{\text{in}}$. In this low frequency limit the contributions of the differential terms in Eq. (1) become negligible, resulting in the relation $\omega_p^2 E_p \approx -A \times E_{\text{in}}$. Substituting $E_p \approx -E_{\text{in}}$ we find $A \approx \omega_p^2$. For the resonance frequencies considered here this leads to values for A that are of the order of 10^{31} s^{-2}.

The electric field associated with the surface plasmon mode at the metal film surface $E_f(t)$ (location 0) is driven exclusively by the E_x component of the field caused by the nanoparticle, and not directly by the incident radiation, due to the large momentum mismatch of the incident light with the surface plasmon waves. The resulting lateral surface plasmon field amplitude at location 0 is described by the following equation:

$$\frac{\partial^2 E_f(t)}{\partial t^2} + \Gamma_f \frac{\partial E_f(t)}{\partial t} + \omega_f^2 E_f(t) = -B[C_{\text{pf}} E_p(t)], \tag{2}$$

where Γ_f is the effective damping constant of the surface plasmon mode in the film, ω_f represents the film resonance frequency in rad/s, C_{pf} again a scaling factor ranging from 0 to 1, here linking the nanoparticle field strength to the resulting surface plasmon driving strength. As was done for parameter A, the approximate magnitude of the constant B can be estimated by considering the low frequency limit. In this limit, we expect that fields at the film surface caused by the particle are approximately cancelled by the film response or $C_{\text{pf}} E_p + E_f \approx 0$. Using this relation we find $B \approx \omega_f^2$. Since $f_f = 4.35\times10^{14}$ Hz, B is approximately of the order of 10^{31} s^{-2}. Note that this analysis does not take into account image charge.

Under harmonic excitation with $E_{\text{in}}(t) = E_{\text{in}}(\omega)e^{-i\omega t}$ it follows that $E_p(t)$ and $E_f(t)$ are of the form $E_m(t) = E_m(\omega)e^{-i\omega t}$ with m either p or f for particle or film, respectively. Substituting these into Eqs. (1) and (2) and solving algebraically to obtain the film and particle field yields

$$E_f(\omega) = -BC_{\text{pf}} \frac{E_p(\omega)}{D_f(\omega)}, \tag{3}$$

and

$$E_p(\omega) = -A \frac{E_{\text{in}}(\omega)}{D_p(\omega)} \left[1 - \frac{ABC_{\text{pf}}C_{\text{fp}}}{D_p(\omega)D_f(\omega)} \right]^{-1}, \tag{4}$$

where $D_m(\omega) = \omega_m^2 - \omega^2 - i\Gamma_m\omega$, with again m either p or f for particle or film, respectively.

To calculate the total field at the positions 0 and 1, we add the relevant contributions of $E_{\text{in}}(\omega)$, $E_p(\omega)$, and $E_f(\omega)$ with appropriate signs and scaling factors. To find the relative sign of these contributions we consider the low frequency limit. Figure 8 shows the relative field direction under low frequency excitation and the corresponding charge distribution in the system. At location 0, the lateral components of $E_p(\omega)$ and $E_f(\omega)$ are opposite, which is accounted for in Eqs. (1) and (2) by the negative sign associated with the parameters A and B. Therefore, the total lateral field at

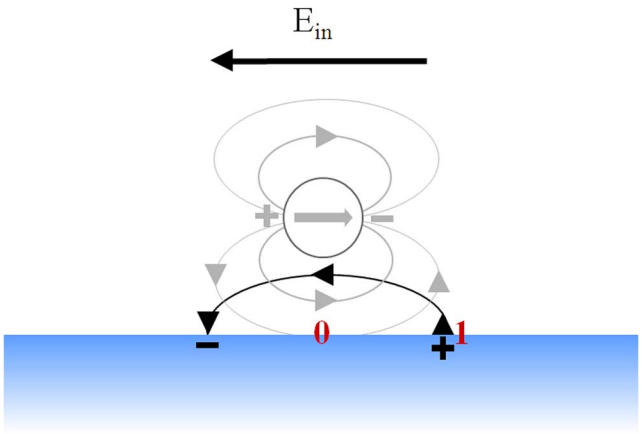

FIG. 8. (Color online) Sketch of the relative orientation of the electric field in the limit of low frequency excitation. The arrow at the top represents the direction of the incident field. The gray lines and arrows represent the field lines associated with the polarized nanoparticle, and the black lines and arrows represent the field lines associated with surface plasmons at the Ag–SiO_2 interface.

location 0 becomes $E_{\mathrm{sum},0}(\omega)=p_0E_{\mathrm{in}}(\omega)+q_0E_p(\omega)+r_0E_f(\omega)$, where p_0, q_0, and r_0 are all positive scaling factors of order 1 that relate the magnitudes of $E_{\mathrm{in}}(\omega)$, $E_p(\omega)$, and $E_f(\omega)$ to their actual contribution at location 0. In contrast, Fig. 8 shows that for the same low frequency field distribution the z-component of the surface plasmon related field at position 1 lies *along* the direction of the z-component of the particle related field. Thus, at location 1, the total normal field is described by $E_{\mathrm{sum},1}(\omega)=p_1E_{\mathrm{in}}(\omega)+q_1E_p(\omega)-r_1E_f(\omega)$, where p_1, q_1, and r_1 are again positive scaling factors of order 1 that relate the magnitudes of $E_{\mathrm{in}}(\omega)$, $E_p(\omega)$, and $E_f(\omega)$ to their actual contribution at location 1. The values of the field scaling constants used are summarized in Table I. The coupling constants were held fixed at $C_{\mathrm{pf}}=C_{\mathrm{fp}}=0.15$, and the damping constants Γ_p and Γ_f were set to 1.7×10^{13} and 9×10^{11} Hz, respectively, to match the FWHM as found in the FIT simulations at AR=3.5.

Figures 9(a) and 9(b) shows the calculated field magnitude using the coupled oscillator model using $A=0.007\omega_p^2$, $B=0.011\omega_f^2$, and $f_f=4.35\times10^{14}$ Hz. The location of f_f is indicated in Figs. 9(a) and 9(b) by the vertical dotted line. The particle resonance frequency was assumed to be identical to that calculated previously for an isolated Ag particle in SiO_2 as marked by the dashed line in Figs. 9(a) and 9(b). Several features that were observed in the full-field simulation results are reproduced by the calculations based on the coupled oscillator model. With the above parameters, the anticrossing between the particle resonance and the film resonance observed in Figs. 6(a) and 6(b) is reproduced in Figs. 9(a) and 9(b). Additionally, the minimum labeled M in Fig. 6(a) is reproduced using the coupled oscillator model [labeled M' in Fig. 9(a)]. The following section discusses the various features observed in Figs. 6(a), 6(b), 9(a), and 9(b).

TABLE I. Constants used in the coupled oscillator model to obtain the electric fields at locations 0 and 1.

Location	E field component	p	q	r
0	x	1.0	0.1	1.0
1	z	0	2.0	3.2

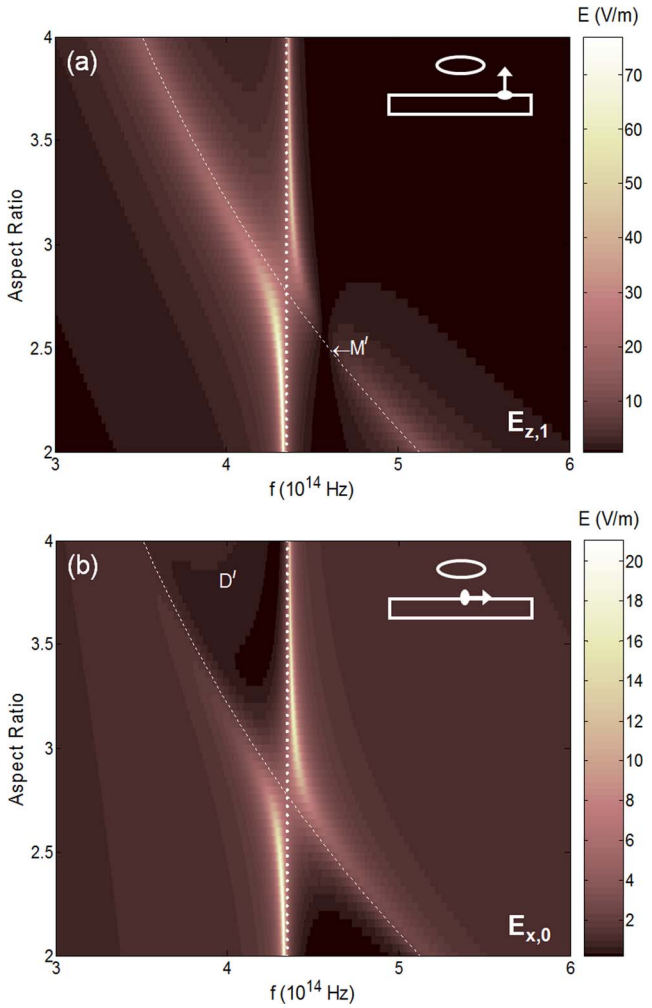

FIG. 9. (Color online) Electric field magnitude (a) $|E_z(f)|$ at location 1, and (b) $|E_x(f)|$ at location 0, as calculated using the coupled oscillator model, for particle aspect ratios in the range of 2–4.

V. DISCUSSION

The coupled oscillator model was shown to reproduce several of the features that were observed in the numerical simulations. This allows us to gain insight into the physical origin of these features. In the following we discuss the origin of the anticrossing, the nature of the sharp minimum in the electric field amplitude above the film resonance frequency, and the origin of the reduced lateral field amplitude at frequencies between the particle and film resonances.

We first consider the observed anticrossing. To understand the nature of the eigenmodes that appear at the aspect ratio where anticrossing is observed, we compare the field amplitudes $E_f(\omega)$ and $E_p(\omega)$ at an aspect ratio of AR=2.9. As seen in Fig. 9(a), this aspect ratio leads to low frequency and high frequency peaks of total field amplitude at $f_L=4.24\times10^{14}$ Hz and $f_H=4.46\times10^{14}$ Hz, respectively. From Eqs. (3) and (4), we can now calculate the relative amplitude of the particle field and the film field. In the low frequency case a particle field amplitude of $E_p(\omega)=+3.21$ V/m and a film

field amplitude of $E_f(\omega)=-4.32$ V/m are obtained, indicating antiparallel alignment of the fields. Conversely, in the high frequency case a particle field amplitude of $E_p(\omega)=+3.09$ V/m and a film field amplitude of $E_f(\omega)=+3.79$ V/m are obtained, indicating parallel alignment of the fields. These antiparallel and parallel field orientations correspond to antiparallel and parallel charge displacements in the particle and film, which agrees well with the eigenmodes obtained using the full field simulations, as shown in Fig. 7.

The observed minimum in E_z [labeled M in Fig. 6(a)] can be understood in terms of the magnitude and phase of the particle and surface plasmon field contributions. Since the nanoparticle provides the only driving force of surface plasmons on the metal film, outside the strong coupling regime the phase of the surface plasmon fields at the film surface approximately follows the behavior of a simple damped driven harmonic oscillator. As a result, the surface plasmon response at the film surface experiences a phase lag relative to the phase of the particle field that varies from $\sim 90°$ under excitation near f_f to $\sim 180°$ when the film is excited well above its resonance frequency. Thus, at frequencies above f_f a condition exists in which the E_z contribution at location 1 by the film is similar in magnitude and *opposite in sign* to that introduced by the nanoparticle. This results in the observed minimum of the total $E_{\mathrm{sum},1}(\omega)$ field at 4.55×10^{14} Hz. Since the nanoparticle drives the charge oscillation in the film, the magnitude of the surface plasmon related field at any frequency is directly proportional to the particle field magnitude at that frequency. Thus the frequency at which cancellation occurs is independent of the specific nanoparticle resonance frequency, as observed near the frequency marked by M and M' in Figs. 6(a) and 9(a).

The region of low field magnitude for frequencies labeled D in Fig. 6(b) is also reproduced by the coupled oscillator model and is labeled D' in Fig. 9(b). This minimum can be understood in terms of the phase and amplitude of the particle field, the excitation signal, and the surface plasmon field. At frequencies above the particle resonance, the lateral field contribution associated with the particle response is finite and approximately *in phase* with the incident field. If these frequencies lie below the resonance frequency of the film, a small surface plasmon amplitude is excited in the film that opposes the particle field. This film response therefore partially cancels the particle field and the incident field near the surface, resulting in the low field amplitude observed in the region labeled D. Note that in the FIT simulations the film response can include contributions from image charges, while in the coupled oscillator model the film response is limited to surface plasmon contributions to the field.

A final observation reproduced by the coupled oscillator model is the appearance of reduced surface plasmon amplitude when the single particle resonance frequency and the film resonance frequency are approximately equal, which leads to the observed anticrossing. This can now be understood in terms of the relative damping of the surface plasmon oscillations on the film and on the nanoparticle. Due to the fact that the damping constant for the dipolar particle resonance is a factor ~ 20 larger than that of the surface plasmons on the Ag film, the largest surface plasmon field amplitude is achieved at relatively small field amplitudes in the particle. In this particular geometry, this occurs at frequencies well away from the particle resonance.

The observations made above have implications for the use of resonant nanoparticles for surface plasmon excitation in finite size arrays. The effective damping of surface plasmons on the silver film can be expected to increase for smaller array sizes as a result of surface plasmons propagating away from the array. Based on the previous analysis we expect that for smaller arrays the optimum surface plasmon amplitude will be reached using a small number of strongly coupled scatterers, while for large arrays the highest surface plasmon field strength will be observed using weakly coupled low-loss scatterers. Future work will involve an investigation of the dependence of surface plasmon excitation efficiency on array size, particle size, as well as particle-surface separation.

Finally, it should be noted that although the coupled oscillator model presented here reproduces many of the features observed in the full-field simulations, it does not take the place of *ab initio* calculations. The strength of the full-field calculations lies in the fact that coupling constants and effective damping constants do not need to be determined independently. The coupled oscillator model on the other hand provides a physical interpretation of the observed features and additionally enables the rapid evaluation of the surface plasmon excitation efficiency for a wide range of geometries by tuning the various model parameters.

VI. CONCLUSIONS

Numerical simulations of a nanoparticle-enhanced plasmon excitation structure consisting of ellipsoidal Ag nanoparticles in close proximity to a $Ag-SiO_2$ interface were presented. It was shown that varying the nanoparticle geometry enables control over the frequency dependent surface plasmon excitation efficiency. Strong coupling between the particle resonance and the film resonance associated with surface plasmons on the silver film was observed as evidenced by anticrossing of the particle and film resonances. It was observed that for the infinitely extended structures simulated here the maximum field amplitude is *not* achieved when the particle resonance frequency and film resonance frequency are matched. These observations were reproduced using a coupled oscillator model and explained in terms of a balance between nanoparticle induced damping and intrinsic surface plasmon damping at the $Ag-SiO_2$ interface. Based on our observations, the optimum geometry for coupling is expected to depend on intrinsic and geometry related damping mechanisms.

ACKNOWLEDGMENTS

This work was supported by the National Science Foundation (CAREER Award ECCS-0644228).

[1] M. L. Brongersma and P. G. Kik, Eds., *Surface Plasmon Nanophotonics* (Springer, Dordrecht, 2007).
[2] H. Raether, *Surface Plasmons on Smooth and Rough Surfaces and on Gratings* (Springer-Verlag, Berlin, 1988).
[3] B. Steinberger, A. Hohenau, H. Ditlbacher, A. L. Stepanov, A. Drezet, F.

R. Aussenegg, A. Leitner, and J. R. Krenn, Appl. Phys. Lett. **88**, 094104 (2006).
[4]J. R. Krenn, B. Lamprecht, H. Ditlbacher, G. Schider, M. Salerno, A. Leitner, and F. R. Aussenegg, Europhys. Lett. **60**, 663 (2002).
[5]D. F. P. Pile, T. Ogawa, D. K. Gramotnev, Y. Matsuzaki, K. C. Vernon, K. Yamaguchi, T. Okamoto, M. Haraguchi, and M. Fukui, Appl. Phys. Lett. **87**, 261114 (2005).
[6]D. K. Gramotnev and D. F. P. Pile, Appl. Phys. Lett. **85**, 6323 (2004).
[7]D. F. P. Pile and D. K. Gramotnev, Opt. Lett. **29**, 1069 (2004).
[8]K. Leosson, T. Nikolajsen, A. Boltasseva, and S. I. Bozhevolnyi, Opt. Express **14**, 314 (2006).
[9]T. Nikolajsen, K. Leosson, I. Salakhutdinov, and S. I. Bozhevolnyi, Appl. Phys. Lett. **82**, 668 (2003).
[10]J. A. Dionne, L. A. Sweatlock, H. A. Atwater, and A. Polman, Phys. Rev. B **73**, 035407 (2006).
[11]J. Krenn and J. Weeber, Philos. Trans. R. Soc. London, Ser. A **362**, 739 (2004).
[12]J.-C. Weeber, Y. Lacroute, and A. Dereux, Phys. Rev. B **68**, 115401 (2003).
[13]J. R. Krenn, H. Ditlbacher, G. Schider, A. Hohenau, A. Leitner, and F. R. Aussenegg, J. Microsc. **209**, 167 (2003).
[14]S. I. Bozhevolnyi, V. S. Volkov, E. Devaux, J. Y. Laluet, and T. W. Ebbesen, Nature (London) **440**, 508 (2006).
[15]T. Nikolajsen, K. Leosson, and S. I. Bozhevolnyi, Appl. Phys. Lett. **85**, 5833 (2004).
[16]W. L. Barnes, A. Dereux, and T. W. Ebbesen, Nature (London) **424**, 824 (2003).
[17]A. Bouhelier and G. P. Wiederrecht, Phys. Rev. B **71**, 195406 (2005).
[18]H. Ditlbacher, J. R. Krenn, N. Felidj, B. Lamprecht, G. Schider, M. Salerno, A. Leitner, and F. R. Aussenegg, Appl. Phys. Lett. **80**, 404 (2002).
[19]H. Ditlbacher, J. R. Krenn, G. Schider, A. Leitner, and F. R. Aussenegg, Appl. Phys. Lett. **81**, 1762 (2002).
[20]G. Webb-Wood, A. Ghoshal, and P. G. Kik, Appl. Phys. Lett. **89**, 193110 (2006).
[21]N. Fang, Z. Liu, T. J. Yen, and X. Zhang, Opt. Express **11**, 682 (2003).
[22]H. Ditlbacher, J. R. Krenn, A. Hohenau, A. Leitner, and F. R. Aussenegg, Appl. Phys. Lett. **83**, 3665 (2003).
[23]A. Ghoshal, G. Webb-Wood, C. Mazuir, and P. G. Kik, Proc. SPIE **5927**, 255 (2005).
[24]N. Papanikolaou, Phys. Rev. B **75**, 235426 (2007).
[25]E. X. Jin and X. Xu, J. Quant. Spectrosc. Radiat. Transf. **93**, 163 (2004).
[26]T. Thio, K. M. Pellerin, R. A. Linke, H. J. Lezec, and T. W. Ebbesen, Opt. Lett. **26**, 1972 (2001).
[27]W. Guo Ping, Y. Yongxiang, and W. Bing, J. Phys.: Condens. Matter **15**, 8147 (2003).
[28]D. Sarid, Phys. Rev. Lett. **47**, 1927 (1981).
[29]C. F. Bohren and D. R. Huffman, *Absorption and Scatterring of Light by Small Particles* (Wiley, New York, 1998).
[30]T. Weiland, AEU **31**, 116 (1977).
[31]Computer code Microwave Studio, Computer Simulation Technology, Darmstadt, Germany.
[32]P. B. Johnson and R. W. Christy, Phys. Rev. B **6**, 4370 (1972).
[33]G. Veronis and S. Fan, in *Surface Plasmon Nanophotonics*, edited by M. L. Brongersma and P. G. Kik (Springer, Dordrecht, 2007), p. 268.
[34]C. Soennichsen, T. Franzl, T. Wilk, G. Plessen, and J. Feldmann, New J. Phys. **4**, 93.1 (2002).